

Tuning the guest-induced spatiotemporal response of isostructural dynamic frameworks towards efficient gas separation and storage

Kornel Roztocki*^[a], Szymon Sobczak^[a,b], Arkadiusz Smaruj^[a,b], Anna Walczak^[a,b], Mateusz Goldyn^[a], Volodymyr Bon^[c], Stefan Kaskel^[c], Artur R. Stefankiewicz*^[a,b]

[a] Faculty of Chemistry, Adam Mickiewicz University, Uniwersytetu Poznańskiego 8, 61-614 Poznań, Poland

[b] Center for Advanced Technology, Adam Mickiewicz University, Uniwersytetu Poznańskiego 10, 61-614 Poznań, Poland

[c] Chair of Inorganic Chemistry, Technische Universität Dresden, Bergstrasse 66, 01062 Dresden, Germany

Table of Contents

Table of Contents.....	1
Experimental Procedures.....	2
Figures.....	5
Tables.....	10
Literature.....	11

Figures

Figure S1 Optical images of single-crystal of UAM-1O (left) and UAM-1S (right) materials.	5
Figure S2 Comparison of single-crystal structure of as synthesized UAM-1O (left) and UAM-1S indicating different pore geometry.	5
Figure S3 First indication of flexibility: comparison IR spectra (first row) and PXRD patterns (second row) of UAM-1O and UAM-1S before (black) and after desolvation (red).....	6
Figure S4 SEM images of MOFs samples after constitutive multicomponent experiments for CO ₂ /CH ₄ mixtures in UAM-1S (left) and in UAM-1S (right). Those samples were further use for <i>in situ</i> experiments. Comparable size of crystals in both sample indicates that different kinetics is not caused by this factor.	6
Figure S5 Comparison CO ₂ isotherms collected at 195K for as synthesized and grounded UAM-1O. ..	7
Figure S6 Optical images and schematic drawing of the customized experimental setup used for the experiments.....	7
Figure S7 Comparison of Thermal stability UAM-1O (red) UAM-1S (black), the chart shows the percentage of weight loss. Before experiment samples were stored for more than 48h at ambient conditions.....	8
Figure S8 IR-ATR spectra of as synthesized frameworks. UAM-1O (red) UAM-1S (black).....	8
Figure S9 PXRD patterns of UAM-1O and UAM-1S stored at ambient conditions. Data set indicates that both materials are stable and UAM-1S has tendency to spontaneous transformation from <i>op</i> to <i>cp</i> phase.	9
Figure S10 Humidity stability of UAM-1X proved by repeatable adsorption and desorption of water vapor at 298K. Data shows that materials are stable in humid conditions.	9

Tables

Table S1 Crystal data and structure refinement for UAM-1S and UAM-1O.....	10
Table S2 Numerical data for isothermal multicomponent adsorption for different CO ₂ /CH ₄ compositions in UAM-1S with corresponding S factor calculated based on eq 1. For more details please see Figure 4.	10
Table S3 Selectivity factor (S) of CO ₂ /CH ₄ for various MOFs, zeolites and activated carbon.....	11

Experimental Procedures

General Remarks. All reagents and solvents were of analytical grade (Sigma Aldrich, Merck, FluoroChem) and were used without further purification. Unless otherwise stated, all manipulations were done under ambient conditions.

Synthesis of 2,5-di (4-*pridyl*)thiazolo[5,4-*d*]thiazole (L) Anhydrous DMF (25 mL) was poured into a round bottom flask. Then added dithioamide (500 mg; 4.6 mmol), and 4-pyridinecarbaldehyde (1071 mg; 10 mmol). Reaction system degassed and placed under an argon atmosphere. The reaction was heated under a cooler in refluxing DMF for 3h, during which time the solution changed color red to brown red, with precipitation of a light yellow precipitate. After the reaction, the solution filtered hot on a Buchner funnel. The precipitate was washed with 20 mL DMF followed by 20 mL EtOH. The precipitate was dried for 24 hours at 80°C. **900 mg (74%)** of a yellow product was obtained. ¹H-NMR (300MHz, CDCl₃): 8.72 (4H, d), 7.82(4H, d).

Synthesis of 4,4'-thiobenzoic acid 4-iodobenzoic acid (12.00 g; 48.4 mmol), anhydrous K₂CO₃ (3.36 g; 24.3 mmol) was poured into a round bottom flask and 48 mL of ethylene glycol was added. The system was heated until the substrates were dissolved. Then Na₂S · 9H₂O (6.38 g; 26.6 mmol) and CuI (0.92 g; 4.8 mmol) were added. The solution was heated under argon to the reflux temperature of the solvent for 24 hours. Then 180 mL of distilled water and activated carbon (4.00 g) were added, and the system was heated under reflux for 10 minutes. The mixture was filtered hot to 30 mL of 6N HCl, the resulting white precipitate was filtered and recrystallized from a propionic acid. The product was dried for 12 hours at 120 °C (7.2 g; 54%). ¹H-NMR (300 MHz, DMSO-*d*₆): 13.08 (2H, s), 7.93 (4H, d), 7.45 (4H, d).

Synthesis of UAM-IX DMF (60 mL) and 100 mg (0.34 mmol) 2,5-di (4-*pridyl*) thiazolo (5,4-*d*) thiazole were added into the reaction vessels. The reaction vessels were sealed and heated in an oven for 5h at 120 °C to dissolve the ligand. After that time, 183.6 mg (0.68 mmol) zinc nitrate tetrahydrate was added to both reaction vessels. To the first vessel 4,4'-oxydibenzoic acid 175.4 mg (0.68 mmol) and to the second 186.4 mg (0.68 mmol) of 4,4'-thiodibenzoic acid were added. The sealed vessels were placed in the oven at 120 °C / 24h. After that time, the crystals were washed with DMF and left in the DMF solution. **Bulk synthesis** was done analogically but the quantity of reagents was increased to 150 ml of DMF, 400mg of (L), 734 mg of zinc nitrate tetrahydrate 703 mg 4,4'-oxydibenzoic acid and 746 mg 4,4'-thiodibenzoic acid. Yield: 927 mg UAM-1O (29%) and UAM-1S 842 mg (28%).

X-ray Crystallography The structural studies for UAM-1S and UAM-1O were performed using an Oxford Diffraction SuperNova diffractometer equipped with a CCD detector and a Cryojet cooling system. X-ray data were collected at 130/132 K using a graphite-monochromated Cu K α radiation source ($\lambda = 1.54178 \text{ \AA}$) with the ω -scan technique. Data reduction, UB-matrix determination, and absorption correction were performed using the CrysAlisPro software.¹ Reciprocal space analysis for UAM-1O in CrysAlisPRO showed that the crystal used for the measurement was a non-merohedral twin.¹ The twin law -1 0 0 0 -1 0 0.25 0 1 corresponds to a 180° rotation about the [001] reciprocal lattice direction. Using Olex2,² the structures were solved by direct methods with ShelXT³ and refined by full-matrix least-squares against F² with the SHELXL refinement package⁴ based on Least Squares minimization. The refinement process for UAM-1O was performed using reflection data in HKLF5. In the refinement process, the reflections from the larger domain that did not overlap with the reflections originating from the smaller component were included. BASF parameters were refined at 0.503(1). All non-hydrogen atoms were refined anisotropically, while the H-atoms were located in idealized positions by molecular geometry and refined as riding groups with Uiso(H) = 1.2Ueq(C). Selected structural parameters are reported in **Table S1**.

Solvent molecules in UAM-1S and UAM-1O were identified on the difference Fourier map. In the UAM-1S structure, two DMF molecules were present, and one of their methyl groups was disordered over two positions. In the UAM-1O structure, six out of seven DMF molecules, whose positions were derived from the Fourier density map, were introduced into the structure model as rigid groups using the FragmentDB tool in Olex2. EADP geometrical constraints were applied to some of them, and two solvent molecules were refined with fixed occupancies of 0.5. In one of the DMF molecules, methyl groups were disordered over two positions. Refinement details are included in the deposited .cif files.

The data have been deposited in the Cambridge Crystallographic Data Collection (CCDC) with deposition numbers CCDC 2247315 and 2247321. These data can be obtained free of charge via www.ccdc.cam.ac.uk/data_request/cif, by emailing data_request@ccdc.cam.ac.uk, or by contacting The Cambridge Crystallographic Data Centre, 12 Union Road, Cambridge CB2.

NMR spectra were recorded on a Bruker Ultrashield 300 MHz spectrometer.

IR spectra were recorded on Thermo Scientific Nicolet iS50 spectrometer with ATR accessory.

Thermogravimetric analyses (TGA) were performed on a setys 1200 setaram instrument at a heating rate of 10 °C min⁻¹ in a temperature range of 20 – 450 °C (approx. sample weight of 40 mg). The measurements were carried out at atmospheric pressure under flowing nitrogen.

Elemental analysis was carried out by conventional microanalysis with the use of an Elementar Vario MICRO Cube elemental analyser

Powder X-ray diffraction (PXRD) patterns were recorded on a Bruker AXD D8 Advance diffractometer with Cu-K α radiation ($\lambda = 1.5418 \text{ \AA}$) in a 2θ range from 3° to 40° with a 0.02° step at a scan speed of 2.5° min⁻¹.

Isothermal adsorption analysis: nitrogen (77 K) and carbon dioxide (195 K) adsorption/desorption studies were performed on a BELSORP-max adsorption apparatus (MicrotracBEL Corp.); 77 K was achieved by liquid nitrogen bath, 195 K was achieved by dry ice/isopropanol bath. Prior to the sorption measurements the samples were soaked 3-4 times in DCM for 3-4h and evacuated at 80 °C for 8-14 h.

Assessing the influence of grinding on adsorption properties of UAM-10. The MOF suspension was transferred to an agate mortar. Excess DMF was filtered off, leaving only a sufficient amount of crystals slightly below the DMF level. The crystals were ground for 3 minutes and then transferred to a screw cap vial. The resulting powder was flooded with 5 ml of DCM. After approximately 2 hours, the DCM was replaced with fresh solvent and left overnight. The following day, the DCM was once again replaced with fresh solvent and left for 2 hours. After this time, the solvent was decanted off, and the powder was gently dried using a dryer. Approximately 50 mg of powder was obtained, put under Ar and sent from Adam Mickiewicz University to TU Dresden. Prior to the sorption measurements the sample was evacuated at 80 °C for 8h. The collected isotherms are presented on **Figure S5**.

High pressure single gas adsorption and mixed gas co-adsorption experiments. Volumetric high-pressure single gas and mixed gas adsorption experiments were conducted using BELSORP-VC (Microtrac MRB) instrument. Helium gas (99.999 % purity) was used for the dead volume measurement. Carbon dioxide (99.999 % purity) and methane (99.999 % purity) gases were used in adsorption experiments. All gases were purchased from Praxair. All isotherms were measured on the same samples ($m_{UAM-10} = 0.652 \text{ g}$; $m_{UAM-1S} = 0.480 \text{ g}$). The DCM@UAM-1X was degassed in dynamic vacuum overnight at 352 K in the measurement cell. Single gas adsorption isotherms were measured at 298 K in the pressure range 52 – 4162 kPa for CH₄ and 0.5 – 5563 kPa for CO₂. Mixed gas adsorption was measured using different gas mixtures of 75 % CO₂ and 25 % CH₄ (v/v) or 50 % CO₂ and 50 % CH₄ (v/v) or 25 % CO₂ and 75 % CH₄ (v/v) at 298 K. The gas mixture composition and adsorption temperatures were chosen because of the pressure limitation of the instrument for gas mixtures. The gas mixture was prepared directly in the standard volume part of the instrument from the pure gases for each point of the isotherm separately. After dynamic mixing of the gases for 60 minutes, the composition of the mixture was determined by the gas chromatograph Agilent 490 Micro-GC-System (GC), coupled to the instrument manifold. The gas mixture was further purged through the sample cell over 60 minutes and overall adsorbed amount was determined from the pressure drop, taking the non-ideality correction for each mixture component into account. The composition of the gas mixture after adsorption was analyzed by GC. To increase the reproducibility of the measurements, 5 GC measurements were done before and after adsorption. The adsorbed amount of mixture components was calculated from the difference in the mixture composition before and after adsorption. Before the measurement of each adsorption point, the sample was degassed in the ultra-high vacuum for 60 minutes at 298 K. For each temperature 5-6 points were measured reaching the maximal equilibrium pressure for the gas mixture of 2215, 3568 and 3258 kPa, respectively for 75 % CO₂ / 25 % CH₄ (v/v), 50 % CO₂ / 50 % CH₄ (v/v) and 25 % CO₂ / 75 % CH₄ (v/v) at 298 K.

Stability tests (Figure S9) The materials have been tested for stability in air conditions. Freshly synthesized materials were left in lab. Process was monitored by PXRD after 2 days, 1 week and 3 weeks. Before 3rd experiments samples were grounded.

Note: All *in situ* experiments were done on a sample used for high pressure single and mix gas adsorption experiments. It assures appropriate crystal size (**Figure S4**) and indicates stability of both frameworks to repeatable adsorption-desorption stress.

In situ powder X-ray diffraction *In situ* PXRD experiments in parallel to gas adsorption were performed on a specialized Empyrean powder X-ray diffractometer (ω - 2θ goniometer, K-Alpha1 system) using a customized setup based on an ARS DE-102 closed cycle helium cryostat for setting up the temperature of the adsorption cell at 195 \pm 0.1 K. The adsorption cell is based on a 1.33" CF-flange and is covered with a beryllium dome. The cell

was connected to the low-pressure port of the BELSORP-max volumetric adsorption instrument. The TTL trigger was used for establishing the communication between BELSORP-max and Empyrean software and ensure the measurement of the adsorption isotherm and PXRD pattern data collection in a fully automated mode. The diffraction experiments were performed using ω - 2θ scans in transmission geometry in the range of $2\theta = 2$ - 70° . The parallel linear Cu $K\alpha_1$ beam, used for the data collection, was obtained by using of the hybrid 2xGe(220) monochromator, 4 mm mask, and primary divergence and secondary antiscatter slits with $1/4^\circ$ opening. A Pixel-3D detector in 1D scanning mode (255 active channels) was used for measurements of reflection intensities. A complete CO_2 adsorption–desorption isotherms at 195 K for **UAM-10** and **UAM-1S** were measured on 42.5 mg and 45.1 mg of the sample correspondingly and PXRD patterns were *in situ* recorded after equilibration (0.1% of pressure change within 300 s) at selected points of the isotherm.

Time-resolved *in situ* PXRD experiments were conducted at P23 *in situ* diffraction and imaging beamline of PETRA III synchrotron (DESY). Monochromatic irradiation with $E = 20.0$ keV ($\lambda = 0.619921$ Å) was used in all experiments. Reflection intensities were measured using a PILATUS 1M (DECTRIS) detector. The distance between the sample and detector is 45 cm. In a typical experiment, PXRD patterns were collected with 10 Hz rate during the 300 – 3600 s.

The experimental setup consists of a volumetric adsorption instrument BELSORP-max (Microtrac MRB), used as gas handling system, which is connected to the customized home-built *in situ* quartz glass capillary ($d = 0.5$ mm) serving as adsorption cell. The capillary was cooled down to 195K using nitrogen cryojet (Oxford Cryosystem 700). The simplified scheme of the setup is given in Fig. S4. The gas dosing system is connected to the *in situ* cell using 1/8 inch stainless tube and the cell was degassed in a dynamic ultra-high vacuum for at least 10 min. A gas cylinder with carbon dioxide (99.999%) was connected to the gas handling system. In the standard experiment, carbon dioxide was dosed into the standard volume of the instrument ($V_{sl} \sim 25$ cm³) using pneumatic valve AV2 to build the desired gas pressure. In the next step measurement of the PXRD patterns was started simultaneously with opening of the valve AV3. The pressures in the standard volume part and in the cell were monitored using electronic manometers P1 and P2. After the experiment, the cell was evacuated by opening the pneumatic valve AV4. In the typical experiment, carbon dioxide pressure of 120 kPa was built up in the standard volume part while the cell was evacuated to $p \leq 1$ Pa. The AV3 valve was opened with delay of 1 second after starting the time-resolved PXRD data collection with a frame frequency of 100 Hz. Typically, the pressure of 60 kPa was registered in the cell after the opening of AV3.

In this work, we used CO_2/CH_4 selectivity factor S (**eqn 1; Fig.3**) instead of Ideal Adsorbed Solution Theory (IAST), recommended for rigid materials. For the ~ 50 % content of CH_4 in a single component experiment, we have obtained a very good $S = 10$ at 298 K (**eqn. 1**):

$$S = \frac{n_{\text{CO}_2\text{ads}} \cdot n_{\text{CH}_4\text{gas}}}{n_{\text{CO}_2\text{gas}} \cdot n_{\text{CH}_4\text{ads}}} = 10 \quad (\text{eqn. S1})$$

Here, $n_{\text{CO}_2\text{ads}}$ and $n_{\text{CH}_4\text{ads}}$ denote number of moles adsorbed ($V_{\text{CO}_2} = 112$ cm³/g; $V_{\text{CH}_4} = 11$ cm³/g) under the specified gas composition ($n_{\text{CO}_2\text{gas}}$ and $n_{\text{CH}_4\text{gas}}$; $p_{\text{CO}_2} = 7.5$ bar and $p_{\text{CH}_4} = 7.5$ bar). For calculation based on multicomponent measurement (Fig. 4, main text) please see **Tab. S2**.

Figures

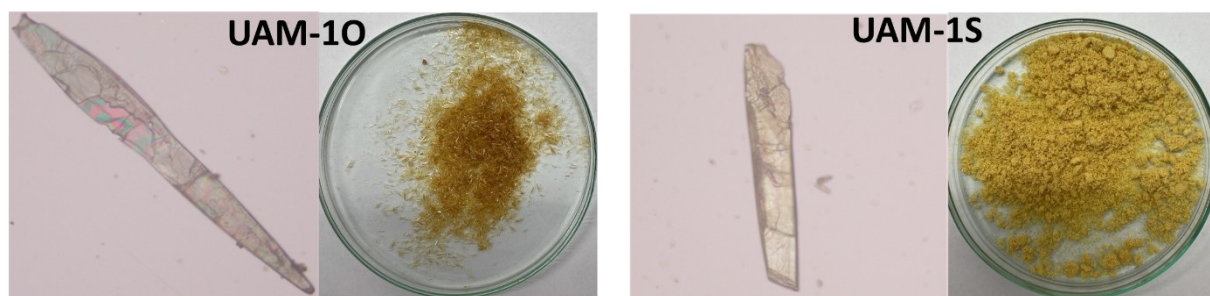


Figure S1 Optical images of single-crystal of UAM-10 (left) and UAM-1S (right) materials.

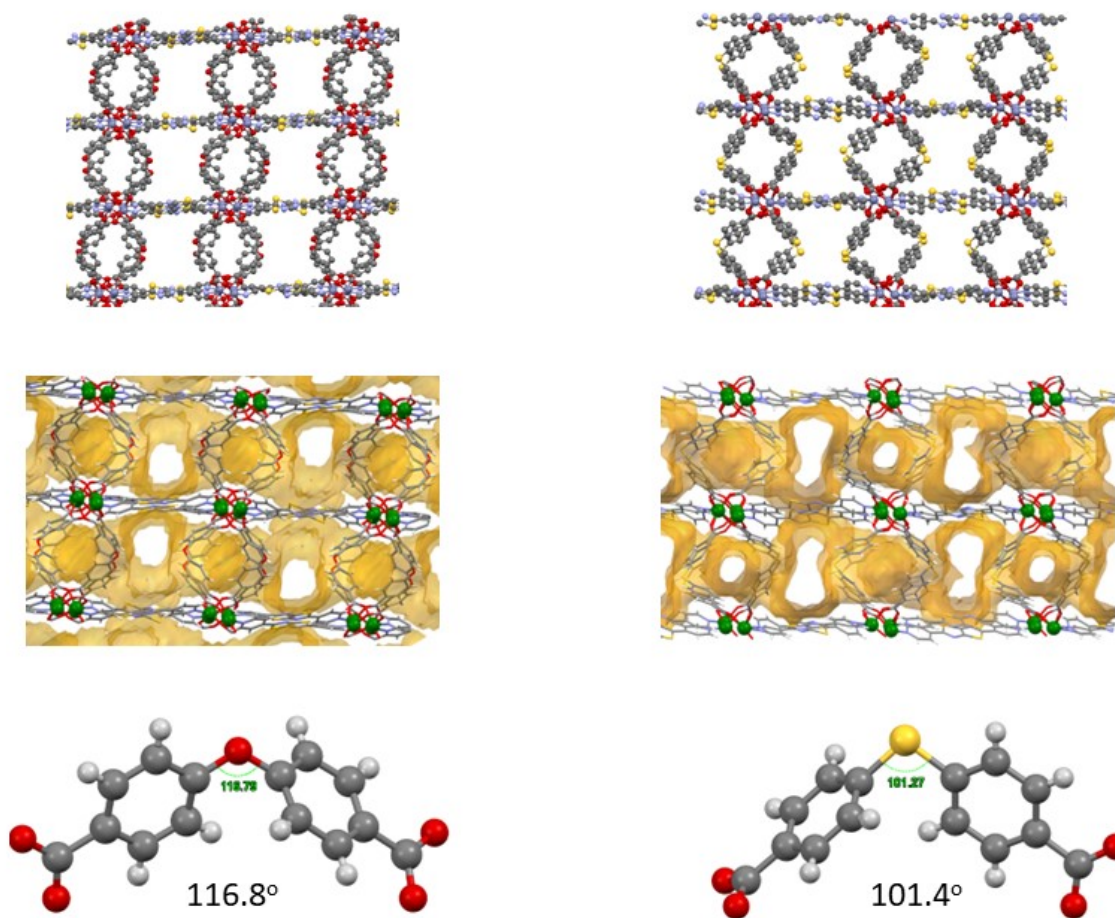


Figure S2 Comparison of single-crystal structure of as synthesized UAM-10 (left) and UAM-1S indicating different pore geometry.

OCO asymmetric stretching region

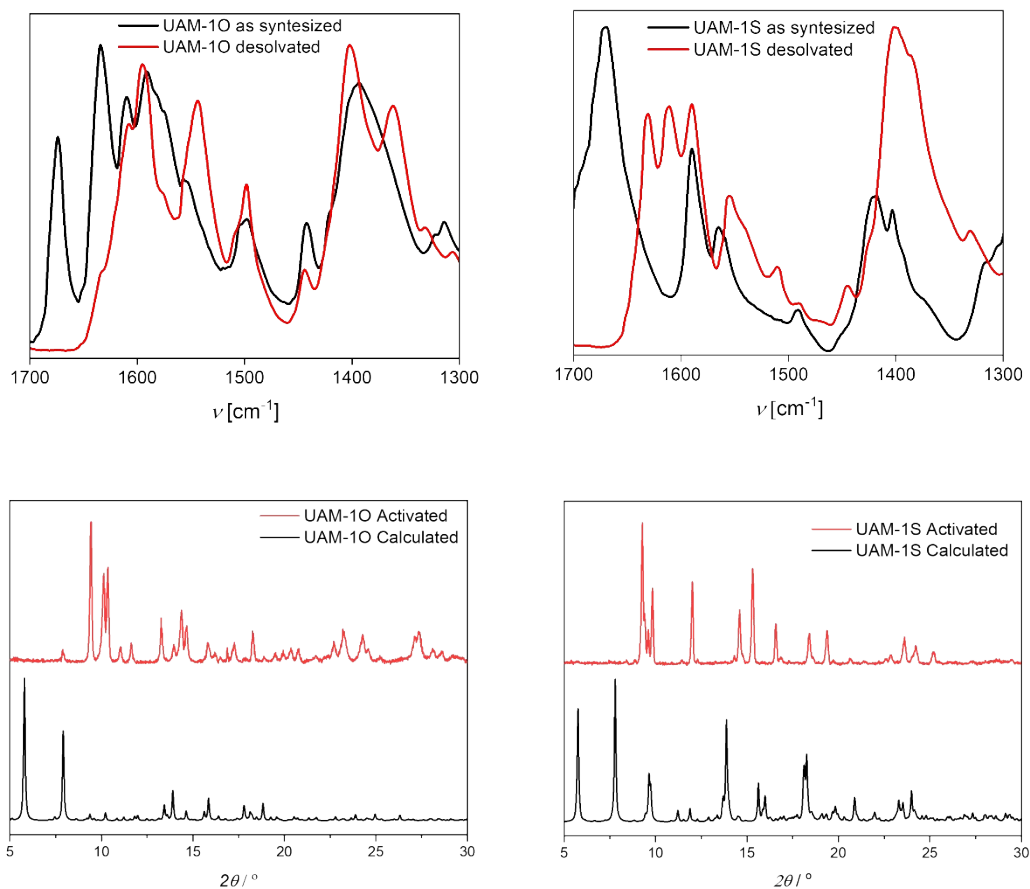


Figure S3 First indication of flexibility: comparison IR spectra (first row) and PXRD patterns (second row) of UAM-1O and UAM-1S before (black) and after desolvation (red).

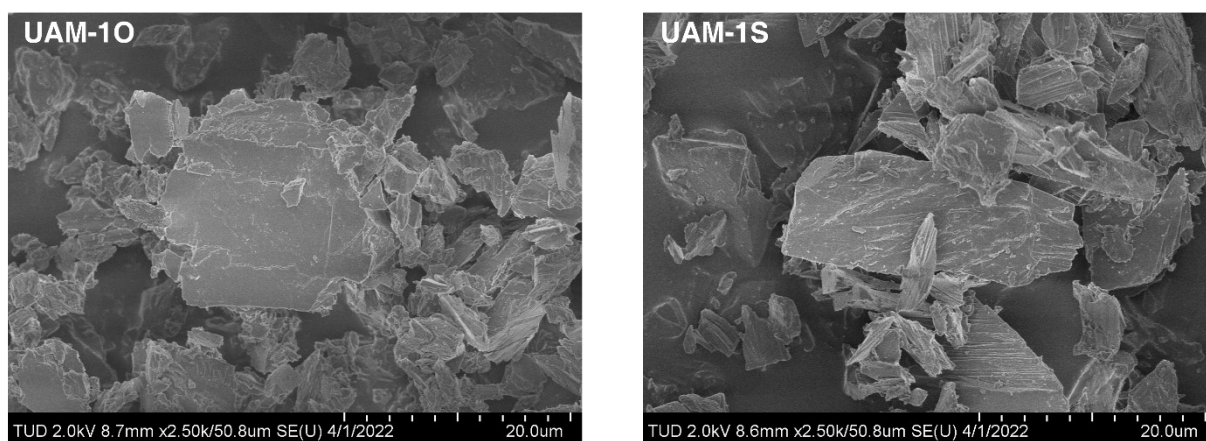


Figure S4 SEM images of MOFs samples after constitutive multicomponent experiments for CO₂/CH₄ mixtures in UAM-1S (left) and in UAM-1S (right). Those samples were further use for *in situ* experiments. Comparable size of crystals in both sample indicates that different kinetics is not caused by this factor.

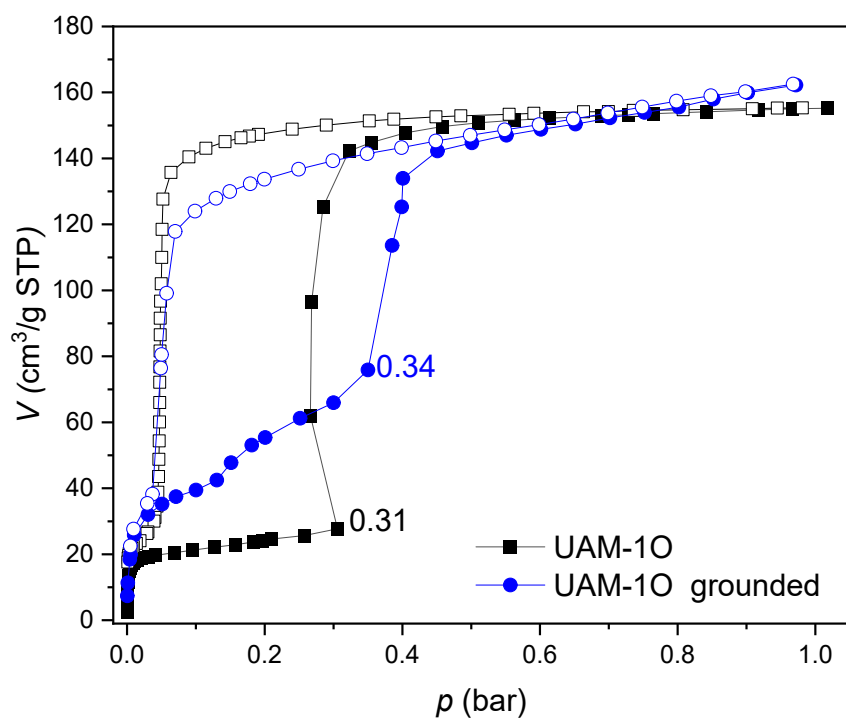


Figure S5 Comparison CO₂ isotherms collected at 195K for as synthesized and grounded UAM-10.

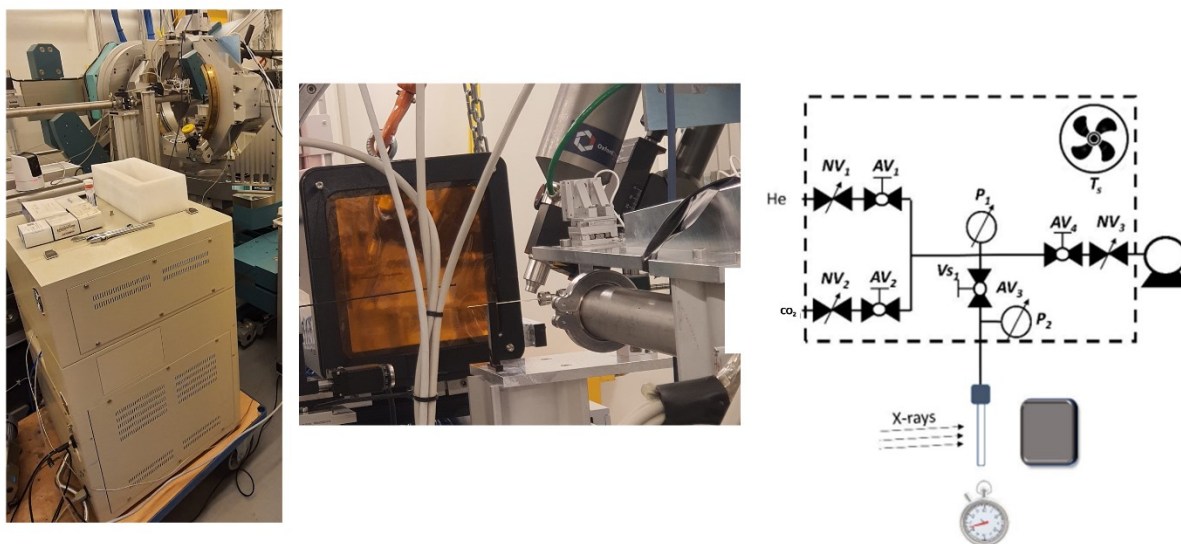


Figure S6 Optical images and schematic drawing of the customized experimental setup used for the experiments.

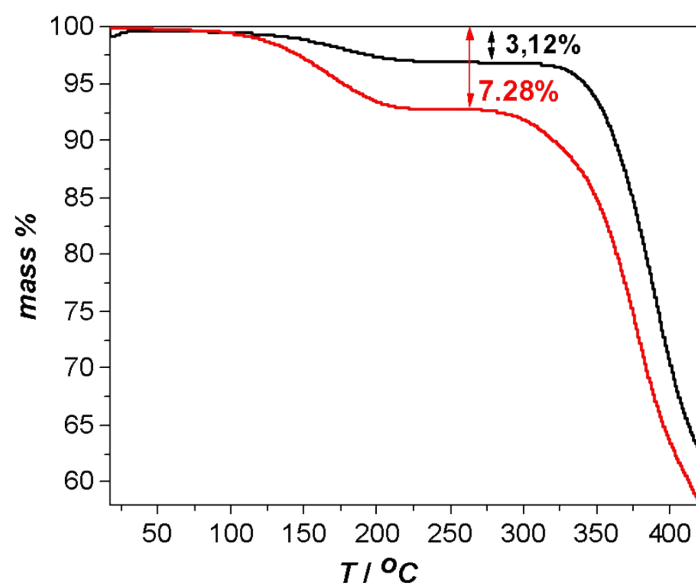


Figure S7 Comparison of Thermal stability UAM-1O (red) UAM-1S (black), the chart shows the percentage of weight loss. Before experiment samples were stored for more than 48h at ambient conditions.

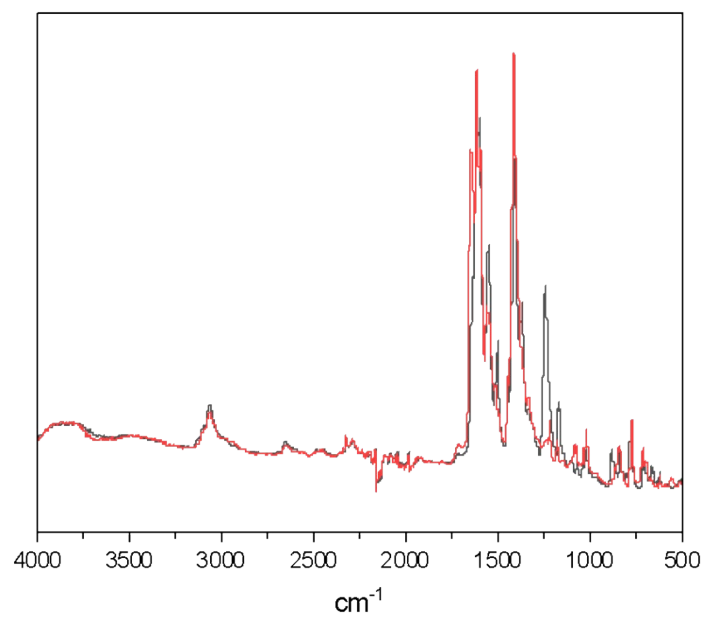


Figure S8 IR-ATR spectra of as synthesized frameworks. UAM-1O (red) UAM-1S (black).

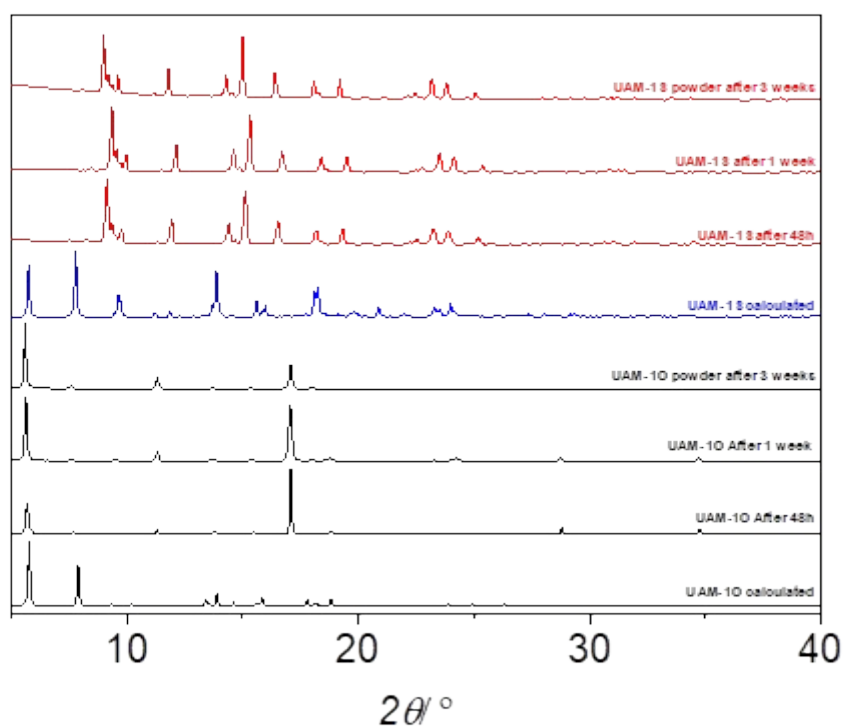


Figure S9 PXRD patterns of UAM-1O and UAM-1S stored at ambient conditions. Data set indicates that both materials are stable and UAM-1S has tendency to spontaneous transformation from *op* to *cp* phase.

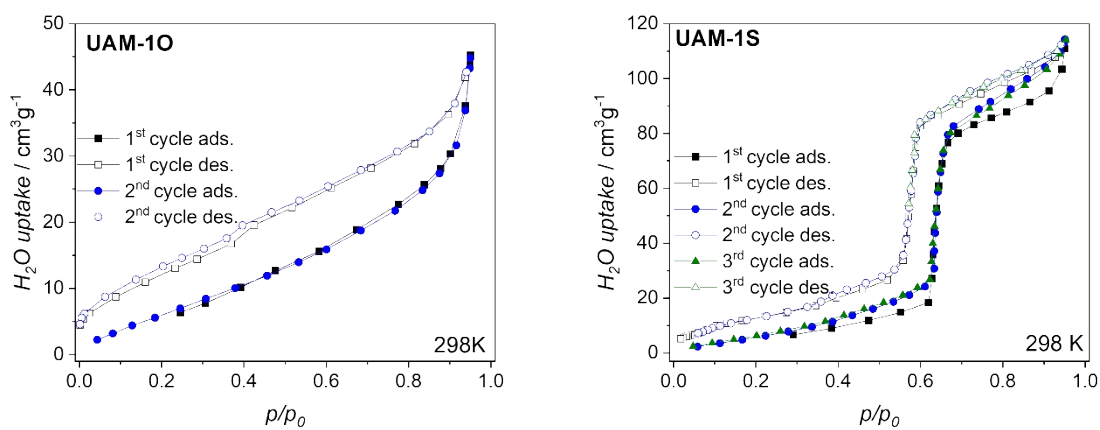


Figure S10 Humidity stability of UAM-1X proved by repeatable adsorption and desorption of water vapor at 298K. Data shows that materials are stable in humid conditions.

Tables

Table S1 Crystal data and structure refinement for UAM-1S and UAM-1O.

	UAM-1S	UAM-1O
Identification code	UAM-1S	UAM-1O
CCDC number	2247315	2247321
Empirical formula	C ₁₀₅ H ₉₇ N ₁₄ O ₂₄ S ₈ Zn ₄	C ₂₀₄ H ₁₈₆ N ₂₈ O ₅₄ S ₈ Zn ₈
Formula weight	2456.92	4758.29
Temperature/K	132.2(2)	129.4(8)
Crystal system	monoclinic	monoclinic
Space group	<i>P2₁/n</i>	<i>P2₁/n</i>
<i>a</i> /Å	22.6778(2)	22.4506(5)
<i>b</i> /Å	16.29760(10)	16.3094(2)
<i>c</i> /Å	30.6684(2)	30.6759(4)
α /°	90	90
β /°	90.6180(10)	95.173(2)
γ /°	90	90
Volume/Å ³	11334.19(14)	11186.4(3)
<i>Z</i>	4	2
ρ_{calc} /cm ³	1.440	1.387
μ /mm ⁻¹	2.969	2.321
<i>F</i> (000)	5060.0	4812.0
Crystal size/mm ³	0.1 × 0.02 × 0.02	0.53 × 0.09 × 0.09
Radiation	CuK α (λ = 1.54184)	CuK α (λ = 1.54184)
2 θ range for data collection/°	5.764 to 152.744	5.786 to 152.82
	-28 ≤ <i>h</i> ≤ 26	-28 ≤ <i>h</i> ≤ 28
Index ranges	-19 ≤ <i>k</i> ≤ 20	-20 ≤ <i>k</i> ≤ 20
	-38 ≤ <i>l</i> ≤ 30	-38 ≤ <i>l</i> ≤ 38
Reflections collected	53098	115138
Independent reflections	23275 [<i>R</i> _{int} = 0.028, <i>R</i> _{sigma} = 0.035]	28382 [<i>R</i> _{int} = 0.047, <i>R</i> _{sigma} = 0.033]
Data/restraints/parameters	23275/0/1432	28382/6/1284
Goodness-of-fit on <i>F</i> ²	1.013	1.072
Final <i>R</i> indexes [<i>I</i> ≥ 2 σ (<i>I</i>)]	<i>R</i> ₁ = 0.0426, <i>wR</i> ₂ = 0.1121	<i>R</i> ₁ = 0.0818, <i>wR</i> ₂ = 0.2341
Final <i>R</i> indexes [all data]	<i>R</i> ₁ = 0.0518, <i>wR</i> ₂ = 0.1195	<i>R</i> ₁ = 0.0913, <i>wR</i> ₂ = 0.2415
Largest diff. peak/hole /eÅ ⁻³	0.74/-0.65	0.90/-0.77

Table S2 Numerical data for isothermal multicomponent adsorption for different CO₂/CH₄ compositions in UAM-1S with corresponding *S* factor calculated based on eq 1. For more details please see Figure 4.

<i>V</i> _{CO2} cm ³ /g	<i>V</i> _{CH4} cm ³ /g	<i>p</i> _{CO2} bar	<i>p</i> _{CH4} bar	<i>S</i>
25:75 CO ₂ :CH ₄				
14.42	3.78	1.12	3.63	12.36
19.98	1.91	2.31	7.37	33.37
33.23	9.31	3.48	11.16	11.45
62.49	29.13	4.57	14.97	7.03
69.57	30.45	4.82	18.99	9.00
77.21	25.77	7.16	23.12	9.67
73.36	29.74	8.02	25.59	7.87
50:50 CO ₂ :CH ₄				
CO2	CH4	<i>p</i> CO2	<i>p</i> CH4	<i>S</i>
52.90	4.16	4.81	4.81	12.72
99.20	11.66	7.23	7.23	8.51
107.62	9.21	9.68	9.69	11.70
111.69	8.57	12.15	12.16	13.04
117.35	5.54	14.68	14.69	21.20
120.28	3.59	17.26	17.29	33.56

75:25 CO ₂ :CH ₄				
CO ₂	CH ₄	pCO ₂	pCH ₄	S
24.31	1.48	3.68	1.23	5.49
101.70	5.36	7.53	2.52	6.35
112.53	4.98	11.70	3.91	7.55
116.63	6.44	16.41	5.48	6.05

Table S3 Selectivity factor (S) of CO₂/CH₄ for various MOFs, zeolites and activated carbon.

Material	S of CO ₂ /CH ₄	T / K	Reference
UAM-1S	see Tab. S2	298	This work
JUK-8	8.83 (20 bar), 5.33 (12 bar) 4.27 (6 bar)	288	5
	9.48 (20 bar), 2.25 (12 bar), 6.6 (6 bar)	293	
	1.99 (20 bar), 3.07 (12 bar), 3.4 (6 bar)	298	
Cu(H-pymo) ₂	1.57 (28 bar)	273	6
MIL-125(Ti)	4.4 (9.8 bar), 6.0 (1 bar)	298	7
	3.1 (9.8 bar), 5.1 (1 bar)	273	
Zn ₂ (bttb)	1.47 (17.5 bar)	298	8
Activated carbon, A35/4	2.2 (1 bar) , 3.39 (9.8 bar)	298	9
CoBDP	64 (58 bar)	298	10

Literature

- (1) Rigaku-Oxford Diffraction; CrysAlisPro Oxford Diffraction Ltd, Abingdon, England V 1. 171. 36. 2. (release 27-06- 2012 CN (2006). Rigaku-Oxford Diffraction; CrysAlisPro Oxford Diffraction Ltd, Abingdon, England V 1. 171. 36. 2. (Release 27-06- 2012 CN (2006).
- (2) Dolomanov, O. V.; Bourhis, L. J.; Gildea, R. J.; Howard, J. A. K.; Puschmann, H. It OLEX2: A Complete Structure Solution, Refinement and Analysis Program. *J. Appl. Crystallogr.* **2009**, *42* (2), 339–341. <https://doi.org/10.1107/S0021889808042726>.
- (3) Sheldrick, G. M. It SHELXT – Integrated Space-Group and Crystal-Structure Determination. *Acta Crystallogr. Sect. A* **2015**, *71* (1), 3–8. <https://doi.org/10.1107/S2053273314026370>.
- (4) Sheldrick, G. M. Crystal Structure Refinement with SHELXL. *Acta Crystallogr. Sect. C Struct. Chem.* **2015**, *71* (Pt 1), 3–8. <https://doi.org/10.1107/S2053229614024218>.
- (5) Roztocki, K.; Rauche, M.; Bon, V.; Kaskel, S.; Brunner, E.; Matoga, D. Combining In Situ Techniques (XRD, IR, and ¹³C NMR) and Gas Adsorption Measurements Reveals CO₂-Induced Structural Transitions and High CO₂/CH₄ Selectivity for a Flexible Metal–Organic Framework JUK-8. *ACS Appl. Mater. Interfaces* **2021**, *13* (24), 28503–28513. <https://doi.org/10.1021/acsami.1c07268>.
- (6) Galli, S.; Masciocchi, N.; Tagliabue, G.; Sironi, A.; Navarro, J. A. R.; Salas, J. M.; Mendez-Liñan, L.; Domingo, M.; Perez-Mendoza, M.; Barea, E. Polymorphic Coordination Networks Responsive to CO₂, Moisture, and Thermal Stimuli: Porous Cobalt(II) and Zinc(II) Fluoropyrimidinolates. *Chem. – Eur. J.* **2008**, *14* (32), 9890–9901. <https://doi.org/10.1002/chem.200801048>.
- (7) Rada, Z. H.; Abid, H. R.; Shang, J.; He, Y.; Webley, P.; Liu, S.; Sun, H.; Wang, S. Effects of Amino Functionality on Uptake of CO₂, CH₄ and Selectivity of CO₂/CH₄ on Titanium Based MOFs. *Fuel* **2015**, *160*, 318–327. <https://doi.org/10.1016/j.fuel.2015.07.088>.
- (8) Bae, Y.-S.; Farha, O. K.; Hupp, J. T.; Snurr, R. Q. Enhancement of CO₂/N₂ Selectivity in a Metal-Organic Framework by Cavity Modification. *J. Mater. Chem.* **2009**, *19* (15), 2131–2134. <https://doi.org/10.1039/B900390H>.
- (9) Heuchel, M.; Davies, G. M.; Buss, E.; Seaton, N. A. Adsorption of Carbon Dioxide and Methane and Their Mixtures on an Activated Carbon: Simulation and Experiment. *Langmuir* **1999**, *15* (25), 8695–8705. <https://doi.org/10.1021/la9904298>.
- (10) Taylor, M. K.; Runčevski, T.; Oktawiec, J.; Bachman, J. E.; Siegelman, R. L.; Jiang, H.; Mason, J. A.; Tarver, J. D.; Long, J. R. Near-Perfect CO₂/CH₄ Selectivity Achieved through Reversible Guest Templating in the Flexible Metal–Organic Framework Co(Bdp). *J. Am. Chem. Soc.* **2018**, *140* (32), 10324–10331. <https://doi.org/10.1021/jacs.8b06062>.